ORGANIC PROCESS RESEARCH & DEVELOPMENT
OPR&D

pubs.acs.org/OPRD

Article

Rate of Formation of Industrial Lubricant Additive Precursors from Maleic Anhydride and Polyisobutylene

Jessica Streets, Nicolas Proust, Dixit Parmar, Gary Walker, Peter Licence, and Simon Woodward*

Cite This: https://doi.org/10.1021/acs.oprd.2c00207

Read Online

ACCESS | Metrics & More | Article Recommendations | Supporting Information

ABSTRACT: The Alder-ene reaction of neat polyisobutylene (**PIB**) and maleic anhydride (**MAA**) to produce the industrially important lubricant additive precursor polyisobutylene succinic anhydride (**PIBSA**) is studied at 150−180 °C. Under anaerobic conditions with [**PIB**] ∼ 1.24 M (550 g mol^{-1} grade, >80% *exo* alkene) and [**MAA**] ∼ 1.75 M, conversion of *exo*-**PIB** and **MAA** follows second-order near-equal rate laws with k_{obs} up to 5 × 10^{-5} M^{-1} s^{-1} for both components. The *exo*-alkene-derived primary product **PIBSA-I** is formed at an equivalent rate. The less reactive olefinic protons of *exo*-**PIB** also react with **MAA** to form isomeric **PIBSA-II** (k_{obs} up to 6 × 10^{-5} M^{-1} s^{-1}). Some *exo*-**PIB** is converted to *endo*-**PIB** (containing trisubstituted alkene) in a first-order process (k_{obs} ∼ 1 × 10^{-5} s^{-1}), while **PIBSA-I** is difunctionalized by **MAA** to bis-**PIBSA**s very slowly. The **MAA**- and **PIB**-derived activation parameter $\Delta G^{\ddagger}$(150 °C) 34.3 ± 0.3 kcal mol^{-1} supports a concerted process, with that of **PIBSA-I** suggesting a late (product-like) transition state.

KEYWORDS: *kinetics, ene reaction, thermal, mechanism, energetics, lubricant*

INTRODUCTION

Lubricating oils and emulsifiers are important global additives with a myriad of technological applications. The total global dispersant market (2021) has been valued at >$6 billion.[1] Polyisobutylene succinic anhydride (**PIBSA**, Scheme 1) occupies a critical market position in the automotive sector and is manufactured on bulk scales (>10^4 tons per year) with an estimated 2022 value of ca. $1.5 billion.[2] Presently, most **PIBSA** is attained by a direct thermal reaction of α-olefin-terminated polyisobutylene (**PIB**) and maleic anhydride (**MAA**) (Scheme 1).[3−5] This reaction is believed to proceed via a classical (uncatalyzed) Alder-ene reaction[3,6] and requires high temperatures (>150 °C) and long reaction times (>20 h) even when the neat reagents are combined.

Scheme 1. Industrial Preparation of PIBSA-I (R = Polymer Chain) and Calculated[7] Model ene Transition State (A, R = *t*-Bu), Showing Interatomic Distances in Å

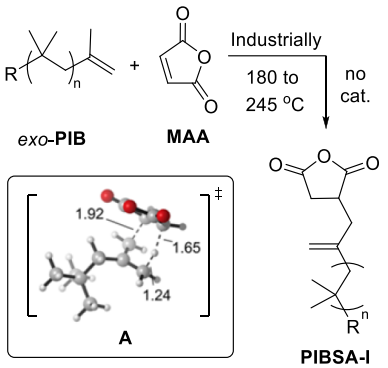

Although the reaction is industrially valuable, the vigorous reaction conditions associated with the industrial process have largely precluded quantitative mechanistic rate investigations. Such investigations could offer insights into how to reduce the present demanding reaction times and temperatures used in current generation industrial **PIBSA** plants. As it is produced at bulk scales under vigorous conditions, small increases in the reaction efficiency disproportionally improve the environmental credentials of the reaction in terms of reduced carbon footprint and related UN sustainable development goals.[8] Even in the most general sense, studies of the kinetics of the Alder-ene reaction are surprisingly limited, and all of these have been carried out under dilute solvent-based conditions, which are unrepresentative of the true industrial process.[6,9,10] Additionally, there are ad hoc observations from production runs that the **PIB**/**MAA** Alder-ene reaction is rather sensitive to the presence of traces of oxygen (or other radical promotors), leading to the formation of alternative products via different mechanisms.[3,4,6,11] A recent (2021) computational study modeled a concerted Alder-ene [4 + 2] pericyclic transition state (**A**) between **MAA** and 2,4,4-trimethylpent-1-ene (*t*-BuCH$_2$C(=CH$_2$)Me), as a surrogate for the end of a **PIB** chain (Scheme 1).[7] This study provided a calculated Gibbs activation energy of 36.6 kcal mol^{-1} (at 150 °C) with an associated enthalpy change ($\Delta H^{\ddagger}$) of 15.8 kcal mol^{-1}. A similar activation barrier (36.7 kcal mol^{-1}) has been calculated (2021)

Received: June 30, 2022

for the uncatalyzed ene reaction between propene and but-3-en-2-one.[12] Both of these papers[7,12] suggest that a significant rate acceleration should be realized in the presence of $AlCl_3$ due to Lewis acid catalysis. We were, therefore, interested in contrasting the theoretical energy barrier for the uncatalyzed reaction to those attained experimentally under conditions that closely simulate the industrial process. Herein, we describe a detailed kinetic study of the direct thermal reaction of **PIB** with **MAA** and comment briefly on the effect of small amounts of $AlCl_3$ on the reaction. The true industrial thermal "ene" synthesis is more complex than the headline summary of Scheme 1. A cascade of competing processes (Scheme 2) occurs during the overall production of **PIBSA**.

Scheme 2. Full Product Distribution of Species Formed in Industrial PIBSA Production (R = Polymer Chain)

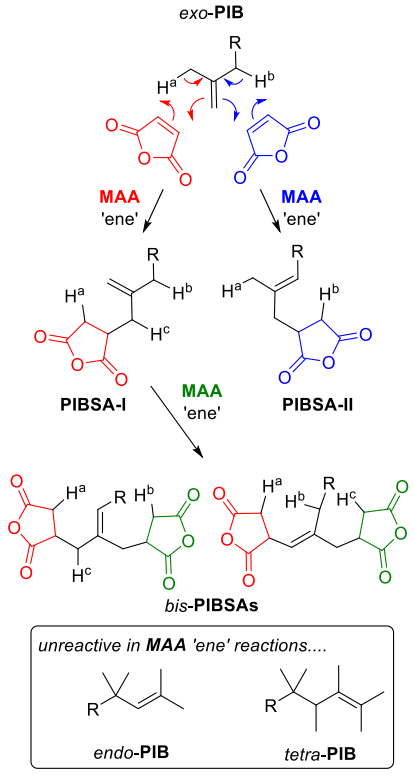

Typically, high vinylidene **PIB** is used in industrial synthesis, containing >80% α-olefin-terminated **PIB** (*exo*-**PIB**), with the remaining composition being β-olefins (*endo*-**PIB**, >10%) and some tetra-substituted alkenes (tetra-**PIB**). These latter two alkenes are not active in Alder-ene chemistry. However, the allylic protons of *exo*-**PIB** (H^a and H^b in Scheme 2) react with **MAA** to generate isomeric **PIBSA-I** and **PIBSA-II**, respectively. Further reaction of equivalent allylic protons (labelled H^b and H^c) within **PIBSA-I** lead to the formation of the bis-**PIBSA** structures shown. Fortunately, although conformation-induced peak broadening and some overlaps occur, diagnostic ^{1}H NMR peaks of all the species within Scheme 2 are available and assigned from the literature precedent,[3] allowing their complete quantification as a function of time. Tetra-**PIB** cannot be monitored by NMR during **PIBSA** synthesis due to the overlap of assigned NMR peaks with those of product **PIBSAs**.

RESULTS AND DISCUSSION

Monitoring of reactions of neat **PIB** and **MAA** is complicated by three factors: (i) **MAA** is only readily soluble in **PIB** above ca. 100 °C and separates stochastically on rapid cooling (invalidating aliquot sampling); (ii) **MAA** is volatile and lost to the reaction headspace under the reaction conditions, causing mass balance/reaction homogeneity issues; (iii) competing radical-based reaction pathways are easily[3] promoted by trace amounts of oxygen (air), leading to alternative byproducts. Preliminary studies showed that aliquot sampling from a single vessel led to very poor reproducibility/induction periods. In standard glassware, the major (but batch-dependent) product was **PIBSA-III**, assigned by us as the structure given in Figure 1, on the basis of our NMR data. A regioisomeric structure has

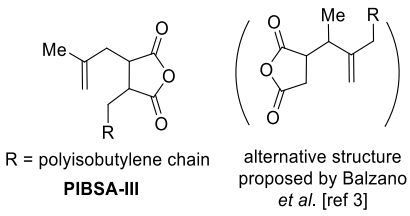

Figure 1. Structure of **PIBSA-III**, a common impurity in aerobic compromised **PIBSA** generation (see also the Supporting Information).

also been proposed by Balzano and co-workers,[3] but in either case, its formation is favored by radical initiators, especially trace oxygen.[11] Such issues have previously prevented accurate kinetic analyses of this reaction, even in the presence of radical inhibitors.[6]

Issues (i)−(iii) were overcome using minimal headspace glass ampoules with Young's tap seals and thorough degassing (see the Experimental Section). By accounting for the different t_1 relaxation values of 550 g mol^{-1} **PIB** and its derivatives versus lighter **MAA** and nitrobenzene NMR standard used, it was possible to obtain quantitative composition-time information from ^{1}H NMR spectra (see the Supporting Information for details) for all **PIB**-containing components. A small series of experiments were conducted to model the background variation in the distribution of **PIB** structures, in the absence of **MAA**, at 150, 165, and 180 °C for 4, 8, 15, 20, and 24 h. No statistically significant variation in the composition occurred, indicating that **PIB** is stable to the reaction conditions in the absence of other components.

Kinetic investigations of the reaction of **PIB** with **MAA** were then completed at 150, 160, 165, 170, and 180 °C, and the composition−time data was extracted by NMR. The nominal molarity of each species was calculated from each spectrum, accounting for the density of **PIB** observed at the experimental temperatures. These results are consistent and reproducible for **PIB** and **PIBSA** species for identical runs (±1−2%), but the quantity of **MAA** present was variable. This variation is due to the poor solubility of **MAA** in **PIB** at room temperature. Although there was no loss of reaction mass, the consumption of **MAA** cannot be monitored by our NMR approach due to its irreproducible precipitation in **PIB** mixtures. The **MAA** content could be quantified by gas chromatography (GC) after solubilizing the total ampoule contents in CH_2Cl_2, although this procedure had a lower reproducibility (ca. 5% error).

https://doi.org/10.1021/acs.oprd.2c00207
Org. Process Res. Dev. XXXX, XXX, XXX−XXX

The experimental concentration−time data are found to best fit the integrated rate laws (1) to (4)[13] for **MAA**, **PIB**, and **PIBSA** species when using nonlinear least squares regression to determine rate constant values (k_{obs}) and goodness-of-fit.[14−16] Statistical analysis of each data set was carried out using SolverStat.[17] This indicated that the second-order near equal concentrations regime best fitted the decay of *exo*-**PIB**, eq 1, and **MAA**, eq 2, and growth of **PIBSA-I** and **PIBSA-II**, eq 3, where $\Delta_0 = [\text{MAA}]_0 - [\text{PIB}]_0$.[13] Growth of *endo*-**PIB** is best modeled using first-order kinetics, eq 4. The observed rate constants, k_{obs}, derived from fitted experimental data for the decay or formation of each species monitored are given in Table 1. Pseudo-first-order rate constants, k_1, necessary for subsequent reaction parameter calculations were obtained by (i) multiplication of k_{obs} (M^{-1} s^{-1}) by $[\textbf{MAA}]_0$ for *exo*-**PIB**, **PIBSA-I**, and **PIBSA-II**, (ii) multiplication of k_{obs} (M^{-1} s^{-1}) by $[\textbf{PIB}]_0$ for **MAA**, and (iii) division of k_{obs} (M s^{-1}) by $[\textbf{MAA}]_0$ for bis-**PIBSAs**. *Endo*-**PIB** forms under first-order conditions, so $k_{obs} = k_1$ (s^{-1}). The worst errors were associated with the formation of bis-**PIBSAs** and *endo*-**PIB** due to their low concentrations, especially at lower temperatures. Interestingly, the generation of *endo*-**PIB** is marginally faster in the presence of **MAA** and **PIBSAs** than in the presence of **PIB** alone. We attribute this to the adventitious generation of trace acid catalyst for C=C bond isomerization.

Table 1. Rate Constants for the Processes of Scheme 2[a]

process	temp (°C)	k_{obs} (M^{-1} s^{-1})	k_1 (s^{-1})
consumption of **MAA**	150	$8(3) \times 10^{-6}$	$1.0(4) \times 10^{-5}$
	160	$3(1) \times 10^{-5}$	$4(1) \times 10^{-5}$
	165	$2(1) \times 10^{-5}$	$3(1) \times 10^{-5}$
	170	$4(1) \times 10^{-5}$	$5(1) \times 10^{-5}$
	180	$5.0(1) \times 10^{-5}$	$6(1) \times 10^{-5}$
consumption of *exo*-**PIB**	150	$3.9(6) \times 10^{-6}$	$7(1) \times 10^{-6}$
	160	$1.6(3) \times 10^{-5}$	$2.8(4) \times 10^{-5}$
	165	$1.7(2) \times 10^{-5}$	$3.0(4) \times 10^{-5}$
	170	$2.6(3) \times 10^{-5}$	$4.5(6) \times 10^{-5}$
	180	$4.1(6) \times 10^{-5}$	$7(1) \times 10^{-5}$
formation of **PIBSA-I**	150	$3(2) \times 10^{-6}$	$5(3) \times 10^{-6}$
	160	$5(4) \times 10^{-6}$	$9(6) \times 10^{-6}$
	165	$1.4(4) \times 10^{-5}$	$2.5(6) \times 10^{-5}$
	170	$2.4(8) \times 10^{-5}$	$4(1) \times 10^{-5}$
	180	$6(1) \times 10^{-5}$	$1.1(3) \times 10^{-4}$
formation of **PIBSA-II**	150	$1.6(6) \times 10^{-5}$	$3(1) \times 10^{-5}$
	160	$5(4) \times 10^{-6}$	$8(7) \times 10^{-6}$
	165	$1(2) \times 10^{-6}$	$1(4) \times 10^{-6}$
	170	$2.1(5) \times 10^{-5}$	$3.6(8) \times 10^{-5}$
	180	$6(1) \times 10^{-5}$	$1.0(2) \times 10^{-4}$

[a]For the formation of *endo*-**PIB** and bis-**PIBSAs**, see the Supporting Information. The number in parentheses is the standard deviation in the preceding digit.

$$[\textit{exo}\text{-}\textbf{PIB}]_t = \frac{\Delta_0[\textit{exo}\text{-}\textbf{PIB}]_0}{\{[\textbf{MAA}]_0 e^{k_{obs}\Delta_0 t} - [\textit{exo}\text{-}\textbf{PIB}]_0\}} \quad (1)$$

$$[\textbf{MAA}]_t = \Delta_0 + [\textit{exo}\text{-}\textbf{PIB}]_0 - [\textbf{PIBSA-I}]_t - [\text{bis-}\textbf{PIBSAs}]_t \quad (2)$$

$$[\textbf{PIBSA}]_t = [\textbf{PIBSA}]_{final}\left(1 - \frac{\Delta_0}{\{[\textbf{MAA}]_0 e^{k_{obs}\Delta_0 t} - [\textit{exo}\text{-}\textbf{PIB}]_0\}}\right) \quad (3)$$

$$[\textit{endo}\text{-}\textbf{PIB}]_t = [\textit{endo}\text{-}\textbf{PIB}]_0 + [\textit{endo}\text{-}\textbf{PIB}]_{final}(1 - e^{-k_{obs}t}) \quad (4)$$

Exact forms of the integrated rate law equation for two consecutive second-order reactions (to simulate the formation of bis-**PIBSA**) are not available.[18] However, due to the significant excess of *exo*-**PIB** and **MAA** compared to bis-**PIBSA**, this reaction became near zeroth order and was modeled as such. Alternative attempts to extract the composite second-order rate constants through Excel-based simulation methods[19] were unsuccessful.

Owing to the occurrence of *exo* to *endo* alkene isomerization, the formation of both **PIBSA-I** and **-II** structures from *exo*-**PIB** and the consumption of **PIBSA-I** to form bis-**PIBSAs** at higher temperatures, all measured components were treated separately. The rate of consumption of **MAA** or **PIB** somewhat exceeds the rate of formation of **PIBSA-I**. This difference is attributed to the accelerated formation of minor species not detected by the NMR assay as the temperature rises and agrees with mass balance loss discussed later. This is also in accord with the minor mass balance issues sometimes noted in plant scale operations over time. A good correlation of the models of eqs 1−4 is attained, with most individual data fits in the range 0.79−0.96 (R^2). This is acceptable and still generates meaningful data, especially considering the challenging

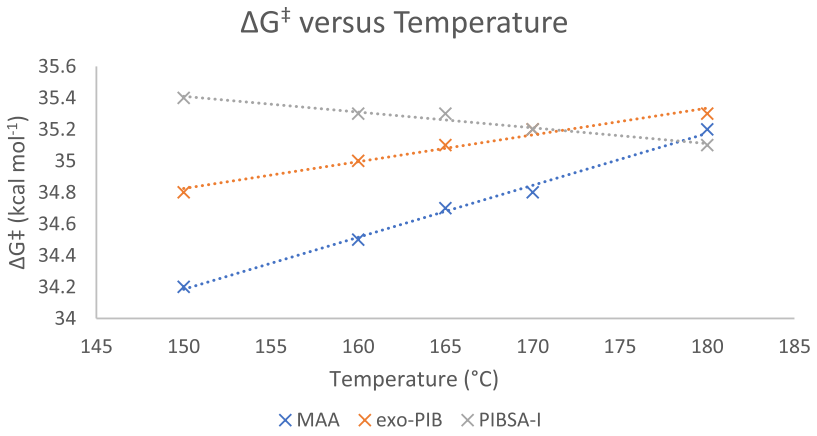

Figure 2. Overall $\Delta G^{\ddagger}$ vs temperature for transformations of Scheme 2 based on **MAA** and *exo*-**PIB** consumption and **PIBSA-I** formation.

https://doi.org/10.1021/acs.oprd.2c00207
Org. Process Res. Dev. XXXX, XXX, XXX−XXX

sampling procedure required. The most significant sources of error are in the GC-based measurement of $[\mathbf{MAA}]_t$ and in the determinations of $[\textit{endo}\text{-}\mathbf{PIB}]_t$ and $[\text{bis-}\mathbf{PIBSA}]_t$ (particularly the latter two, which are only present at low concentrations). Attempts to extend our study above 180 °C were not successful with our present setup.

The Eyring–Polanyi equation (eq 5) allows estimation of the Gibbs free energy of activation ($\Delta G^{\ddagger}$) for a reaction and its deconvolution into $\Delta H^{\ddagger}$ and $\Delta S^{\ddagger}$ (see the Supporting Information). Plotting the derived $\Delta G^{\ddagger}$ values for **MAA**, *exo*-**PIB**, and **PIBSA-I** versus temperature is informative (Figure 2). Both **MAA** and *exo*-**PIB** show increasing $\Delta G^{\ddagger}$ with increasing temperature. Such behavior either indicates significant ordering in the transition state (i.e., a strong negative $\Delta S^{\ddagger}$ term) or that additional reaction manifolds (requiring higher $\Delta G^{\ddagger}$) are becoming available as the reaction temperature increases. Conversely, the $\Delta G^{\ddagger}$ values attained from the rate of **PIBSA-I** formation fall as temperature rises. Even allowing for the experimental error, the difference between $\Delta G^{\ddagger}$ of the starting materials and product is beyond the error bar.

$$k = \frac{k_B T}{h} e^{\Delta S^{\ddagger}/R} e^{-\Delta H^{\ddagger}/RT} \tag{5}$$

While the experimental $\Delta G^{\ddagger}$(150 °C) values from **MAA**, *exo*-**PIB**, and **PIBSA-I** (34.1 ± 1.5, 34.8 ± 2.2, and 35.4 ± 2.2 kcal mol^{-1}, respectively), compare well to those (36.6 kcal mol^{-1}) derived from density functional theory (DFT) studies,[7,12] the relative slopes of Figure 2 point to a more complicated picture. Table 2 presents the Eyring-Polanyi $\Delta H^{\ddagger}$ and $\Delta S^{\ddagger}$ values deconvoluted from the **MAA**, *exo*-**PIB**, and **PIBSA-I** $\Delta G^{\ddagger}$ data. As no literature $\Delta H^{\ddagger}$ or $\Delta S^{\ddagger}$ experimental values are available for individual components of the Alder-ene reaction of **PIB** and **MAA**, Arrhenius plots of each dataset (**MAA**, *exo*-**PIB**, and **PIBSA-I**) were also made (see the Supporting Information) to determine the activation energy (E_a) from each of these components (eq 6 and Table 2).

Table 2. $\Delta H^{\ddagger}$, $\Delta S^{\ddagger}$, and E_a Values from the MAA, *exo*-PIB and PIBSA-I Rate Data[a]

reaction process	$\Delta H^{\ddagger}$ (kcal mol^{-1})	$\Delta S^{\ddagger}$ (eu)	E_a (kcal mol^{-1})
consumption of **MAA**	21(7)	−33(15)	21.6(66)
consumption of *exo*-**PIB**	28(5)	−16(11)	29.0(47)
formation of **PIBSA-I**	40(4)	11(9)	40.9(40)

[a]The number in parentheses is the standard deviation in the preceding digit.

$$k = Ae^{-E_a/RT} \tag{6}$$

Literature activation energies (E_a) of all published Alder-ene reactions using maleic anhydride are presented in Table 3, together with how the values were attained.[9−11] No literature value exists for the **PIB** and **MAA** system for direct comparison; Martuano has attempted this previously but was unable to reproducibly quantify the reaction components using high-performance liquid chromatography or GC methods.[6] The activation energy of the ene reaction between **MAA** and polypropylene (M_n ∼2010 g mol^{-1}, M_w ∼10,300 g mol^{-1}) has been calculated as 22.0 kcal mol^{-1} from an IR-derived rate of consumed **MAA**.[10] These studies[6,9,10] all conclude that **MAA**-ene reactions are first order with respect to both alkene and enophile and second order overall, in line with our own findings. However, as far as we can determine, no previous Eyring analysis of all of the components of an Alder-ene synthesis has previously been undertaken, even though the reaction is 80 years old. While the **PIB** system can be expected to have a slower rate due to the increased steric bulk of the polymeric alkene, the (reproducible) activation parameters of **PIBSA-I** (Table 2) are not in accord with the large-$\Delta S^{\ddagger}$ term seen for classic pericyclic reactions. One potential rationale for the data in Table 2 is that the **MAA** and **PIB** consumption data is "contaminated" by competing higher energy processes. In line with this, some deviation between the calculated reaction composition data and the observed amounts of **PIB** and **MAA** is observed. At 150 °C, 11% of the mass balance is unaccounted for after 24 h. At 180 °C, this figure rises to ca. 30%. We can detect no mass loss from our reactions, implying that depolymerization of **PIB** to isobutylene is not an issue. This indicates the production of additional product(s) undetected by the NMR and GC assays. These products must be insoluble in $CDCl_3$ or be sufficiently line broadened to not have clear NMR peaks. Gel permeation chromatography (GPC) analysis additionally did not reveal any more information, and the mass balance loss does not correlate to the IR signal that has been assigned to poly(maleic anhydride) species.[10] The undetected byproducts are most likely high-molecular-weight solid polymers.

The **PIBSA-I** data in Table 2, if correct, suggests a late (product-like) transition state where the developing C–H bond is already well established. This is in line with the recent (2021) DFT calculations that triggered our investigation.[7,12] In a final comparison with these *in silico* studies, we tested the efficacy of the Lewis acid catalyst $AlCl_3$, which is predicted to provide strong rate acceleration. At loadings of 3–8 mol % (with respect to **PIB**), conversion of **MAA** and **PIB** to **PIBSA-I** and **II** was essentially unaffected compared to the

Table 3. Available Kinetic Data for Alder-ene Reactions Using MAA

alkene	E_a (kcal mol^{-1})	$\Delta S^{\ddagger}$ (eu)	how determined	conditions	ref
4-phenylbut-1-ene	16.1 ± 0.1	−47.3 ± 0.2	**MAA** data alone; GC method	$C_6H_3Cl_3$ solution; excess **MAA**; 4% quinol vs [ene]	6
2,4-dimethyl-4-phenylpent-1-ene	12.5 ± 0.3	−52.8 ± 0.7	**MAA** data alone; GC method	$C_6H_3Cl_3$ solution; excess **MAA**; 7% quinol vs [ene]	6
C_6–C_{10} 1-alkenes	21.5 ± 0.7	−36.4 ± 1.1	averaged k_2 from alkene, **MAA** and product data; GC method	$C_6H_4Cl_2$ solution; 2% quinol vs [ene]	9
trans-dec-5-ene	18.1 ± 1.5	−42.6 ± 3.5	averaged k_2 from alkene, **MAA** and product data; GC method	$C_6H_4Cl_2$ solution; 2% quinol vs [ene]	9
allylbenzene	ca. 20	n/a	**MAA** data alone; titration method	$C_6H_4Cl_2$ solution	11
polypropylene	22.0 ± 2.6	n/a	**MAA** data alone; FTIR method	DMF solution; TEMPO (conc. not specified)	10

https://doi.org/10.1021/acs.oprd.2c00207
Org. Process Res. Dev. XXXX, XXX, XXX−XXX

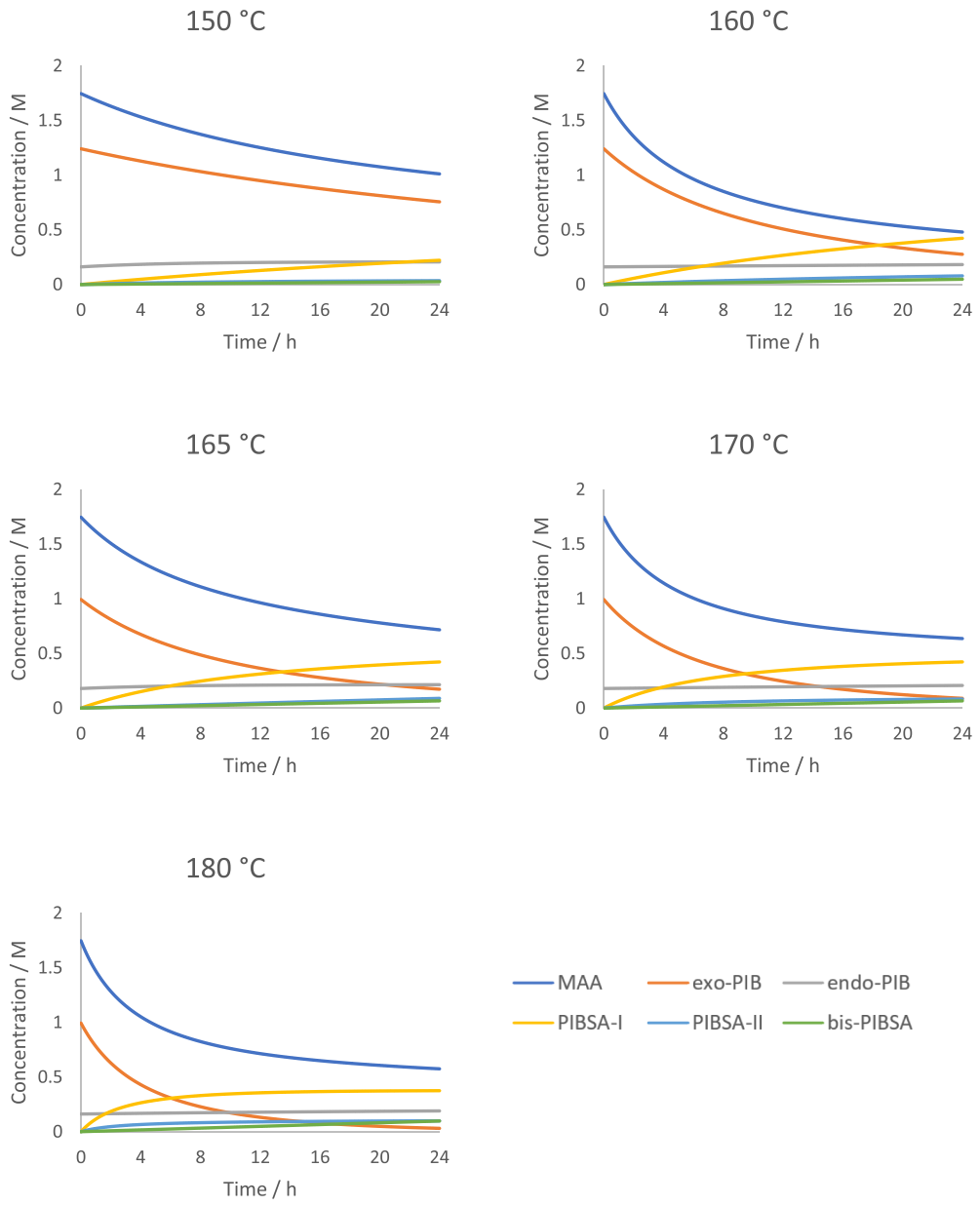

Figure 3. Final simulated reaction composition of the Alder-ene reaction between **PIB** and **MAA** at 150, 160, 165, 170, and 180 °C across 24 h using eqs 1−4 and the data in Table 1.

background reaction. The proportion of *endo*-**PIB** increased compared to uncatalyzed conditions as catalyst loading increased. This outcome is in agreement with the literature that suggests evolution of HCl from catalysts accelerates the *exo*-olefin to *endo*-olefin isomerization.[20] Given the clear calculated drivers for Lewis acid acceleration and the fact that this is a successful strategy in other Alder-ene reactions,[12] it is likely that the minor byproducts affecting the recorded rate data for **MAA** and **PIB** are also strong sequestering agents for $AlCl_3$.

Previous kinetic studies of the ene reaction(see Table 3) have predominately included a radical inhibitor, such as quinol, or a scavenger, such as TEMPO. A smaller series of reactions was conducted with 2% quinol at 165 °C and monitored by our quantitative NMR methods. The rate of consumption of *exo*-**PIB** fell to $1.4(4) \times 10^{-5}$ M^{-1} s^{-1}, which is equal to the rate of formation of **PIBSA-I** in the absence of the radical inhibitor in Table 1. No difference in the rate was observed in the presence of 2% quinol and 5% $AlCl_3$ after 4 h at 150 °C (data in the Supporting Information).

Despite these underlying factors, the models of eqs 1−4 and the rate constants derived here do provide a good model for the **PIBSA** process. Figure 3 shows the calculated reaction composition across 24 h at each of the temperatures studied. These profiles are in good accord with the reaction profiles seen at industrial scales.

CONCLUSIONS

A kinetic model of the Alder-ene reaction of neat **PIB** and **MAA** to produce the industrially produced lubricant precursor **PIBSA** has been developed. Rate data attained from all observable reaction components between 150 and 180 °C can accurately reproduce bulk plant behavior as a function of temperature.[21] Detailed extraction of the key kinetic

https://doi.org/10.1021/acs.oprd.2c00207
Org. Process Res. Dev. XXXX, XXX, XXX−XXX

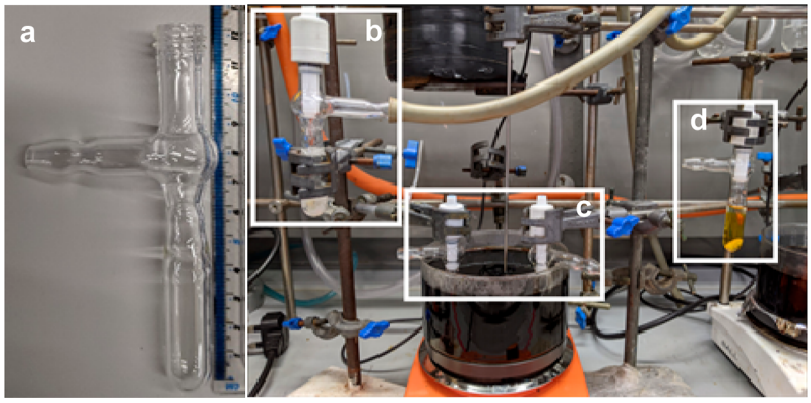

Figure 4. Representative ampoules used in this study: (a) before charging, (b) during degassing, (c) during a typical kinetic run (170 °C), and (d) at the completion of the reaction.

parameters ($\Delta G^{\ddagger}$, $\Delta H^{\ddagger}$, $\Delta S^{\ddagger}$, and E_a) leads to the conclusion that **MAA** and **PIB** are coproducing small amounts of undetected (by NMR, GC, and GPC) byproducts that engender two negative effects. First, this coproduction skews the acquired activation data attained for the process, complicating its analysis, and second, the same byproducts apparently sequester $AlCl_3$ that otherwise would be a good catalyst for the process. Kinetic data from the **PIBSA-I** product of the reaction are unaffected by $AlCl_3$ and point to a late (product-like) transition state, where C−H bond formation is already appreciably developed, as seen in recent computational models. Understanding these features points to the need to develop catalysts that are active well below current **PIBSA** plant operating temperatures, avoiding inhibition of byproduct formation, but using alternative activation modes for **PIB** and/or **MAA**. Such approaches would allow new optimization strategies for this important reaction and provide a significant opportunity to reduce the manufacturing footprint.

Experimental Section. High vinylidene 550 g mol^{-1} molecular weight polyisobutylene (**PIB**) used was of an identical grade to that used for industrial lubricant synthesis (Lubrizol). This **PIB** sample contained 80 mol % α-olefins, 15 mol % β-olefins, and 5 mol % tetra-substituted olefins by ^{1}H NMR spectroscopy; GPC studies confirmed its molecular weight and indicated a polydispersity of M_W/M_n = 1.5. **MAA** was commercial (Alfa Aesar), equivalent to that used in the industrial process; its purity was confirmed as >98% by ^{1}H NMR spectroscopy.

Experimental Set-Up. Kinetic runs were conducted using bespoke pressure-resistant glass ampoules with Young's tap seals (internal diameter, 6 mm; external diameter, 12 mm; height, 120 mm; total volume, 6 mL) (Figure 4). This reaction setup mimics the minimum headspace designs of current industrial **PIBSA** plants and allows multiple duplicate reactions (that give identical conversion-time outputs between batches within ±1−2%) to be set up simultaneously when determining the rates controlling the **PIBSA** cascade (Scheme 2).

Kinetic Runs. Solid **MAA** (0.816 g, 8.32 mmol, 1.4 equiv), a 10 mm stir bar, and **PIB** (3.270 g, 5.95 mmol, 1.0 equiv) were charged to the ampoule, and Young's tap was sealed. The reaction mixture was left to settle for 12−16 h to facilitate degassing, which was achieved by 3× vacuum (1 mbar)/N_2 gas cycles. Young's tap was closed under a flow of N_2, and the ampoule was fully submerged in a preheated oil bath (150, 160, 165, 170, or 180 °C), and the kinetics clock started. Sealed reactions were shielded by a blast screen during heated runs. Individual duplicates of the reactions were stopped hourly to provide data over a 24 h window. Owing to the laboratory (covid) open hour restrictions, no data for 11−13 h periods could be collected. To prevent loss of volatile **MAA**, individual reaction samples were cooled to room temperature before the ampoules were opened. Control runs indicated that nominally identically charged ampoule compositions provided identical conversions at given time points (±1−2% conversion). Independent experimental estimates of the densities of **PIB**−**MAA** mixtures in the temperature ranges studied allow the use of molarity, as opposed to molality, units in the kinetic analyses. Amounts of **MAA** were determined by GC and all other species by ^{1}H NMR spectroscopy (see the Supporting Information for details). Radical inhibitors were not found to be necessary under these conditions and were not used to avoid potential additional rate data being needed. Conversion in the presence of freshly sublimed $AlCl_3$ (3−8 mol % vs PIB) was checked at 150 °C, 4 h and found to be comparable to background conversion within the experimental error (see the Supporting Information). Conversion in the presence of 2% quinol (vs PIB) was calculated at 165 °C at 3, 6, 9, 15, 18, 21, and 24 h and revealed a rate of consumption of *exo*-**PIB** equal to the formation of **PIBSA-I** in the absence of the radical inhibitor (see the Supporting Information).

Data Analyses. Experimental data were fitted to all kinetic models of eqs 1−4 using Solver Microsoft Excel add-in.[14−16] Data fits were optimized by nonlinear least squares regression of the sum of ([observed species] − [calculated species])^2 as a function of k_{obs} and where relevant $[\mathbf{PIBSA}]_{final}$, at fixed $[\mathbf{PIB}]_0$ and $[\mathbf{MAA}]_0$ values. A near equal concentration (second order overall)[13] rate law gave the best fit to the data based on R^2, except for the isomerization of *exo*-**PIB** to *endo*-**PIB** (which fitted first order) and the formation of bis-**PIBSAs** (which was zeroth order). The SolverStat tool was used to return regression statistics on all coefficients, including the standard deviations and R^2 values (see the Supporting Information).[17] Derived parameters (E_a, $\Delta H^{\ddagger}$, $\Delta S^{\ddagger}$, and $\Delta G^{\ddagger}$) were calculated from k_{obs}. The standard deviations for the derived $\Delta G^{\ddagger}$ values were calculated using eqs 7−11. Full details are given in the Supporting Information.

$$\text{Decimal percentage standard deviation in } \Delta H^{\ddagger} \text{ or } \Delta S^{\ddagger} = \frac{\text{std. dev. in } \Delta H^{\ddagger} \text{ or } \Delta S^{\ddagger}}{\text{calculate value of } \Delta H^{\ddagger} \text{ or } \Delta S^{\ddagger}} \quad (7)$$

https://doi.org/10.1021/acs.oprd.2c00207
Org. Process Res. Dev. XXXX, XXX, XXX−XXX

$$\text{Variance in } \Delta H^{\ddagger} \text{ or } \Delta S^{\ddagger} = (\text{standard deviation in } \Delta H^{\ddagger} \textit{ or } \Delta S^{\ddagger})^2 \quad (8)$$

$$\text{Linear combination to calculate } \Delta G^{\ddagger} = \Delta H^{\ddagger} - T\Delta S^{\ddagger} \quad (9)$$

$$\text{Variance in } \Delta G^{\ddagger} = \mathrm{Var}(\Delta H^{\ddagger} - T\Delta S^{\ddagger}) = 1^2(\mathrm{Var}(\Delta H^{\ddagger})) + T^2(\mathrm{Var}(\Delta S^{\ddagger})) \quad (10)$$

$$\text{Standard deviation in } \Delta G^{\ddagger} = \sqrt{\mathrm{Var}(\Delta G^{\ddagger})} \quad (11)$$

All other details and primary data are in the Supporting Information.

■ ASSOCIATED CONTENT

Supporting Information

The Supporting Information is available free of charge at https://pubs.acs.org/doi/10.1021/acs.oprd.2c00207.

Details of GC and NMR kinetic data acquisition procedures; estimates of safe operating pressures for the glass ampoules used; primary data from all runs; and Eyring–Polanyi and Arrhenius plots (PDF)

■ AUTHOR INFORMATION

Corresponding Author

Simon Woodward − *GSK Carbon Neutral Laboratories for Sustainable Chemistry, University of Nottingham, Nottingham NG7 2TU, U.K.;* orcid.org/0000-0001-8539-6232; Email: simon.woodward@nottingham.ac.uk

Authors

Jessica Streets − *GSK Carbon Neutral Laboratories for Sustainable Chemistry, University of Nottingham, Nottingham NG7 2TU, U.K.;* orcid.org/0000-0001-5040-5135

Nicolas Proust − *The Lubrizol Corporation, Wickliffe, Ohio 44092, United States*

Dixit Parmar − *The Lubrizol Corporation, Hazelwood, Derby DE56 4AN, U.K.*

Gary Walker − *The Lubrizol Corporation, Hazelwood, Derby DE56 4AN, U.K.*

Peter Licence − *GSK Carbon Neutral Laboratories for Sustainable Chemistry, University of Nottingham, Nottingham NG7 2TU, U.K.;* orcid.org/0000-0003-2992-0153

Complete contact information is available at: https://pubs.acs.org/10.1021/acs.oprd.2c00207

Notes

The authors declare the following competing financial interest(s): We should declare that the Lubrizol Corporation is a major provider of PIBSA, but none of the authors derive any direct benefits from this.

■ ACKNOWLEDGMENTS

The authors thank the University of Nottingham and the Lubrizol Prosperity Partnership (EPSRC: EP/V037943/1) for facilitating this research. J.S. is grateful to the EPSRC and the SFI Centre for Doctoral Training in Sustainable Chemistry (EP/S022236/1) for a studentship. The authors also thank the referees for their incisive comments and input.

■ REFERENCES

(1) Technavio. *Lubricant Additives Market by End-User and Geography—Forecast and Analysis 2021-2025*, 2021.

(2) Global Polyisobutenyl Succinic Anhydride (PIBSA). Market Insights and Forecast to 2028. https://www.proficientmarketinsights.com/global-polyisobutenyl-succinic-anhydride-pibsa-market-19875020 (accessed Mar 02, 2022).

(3) Balzano, F.; Pucci, A.; Rausa, R.; Uccello-Barretta, G. Alder-Ene Addition of Maleic Anhydride to Polyisobutene: Nuclear Magnetic Resonance Evidence for an Unconventional Mechanism. *Polym. Int.* **2012**, *61*, 1256−1262.

(4) Rausa, R. Synthesis of Polyisobutenyl Succinic Anhydrides. Product Distribution and Proposed Reaction Mechanism. *Polym. Prepr.* **2007**, *48*, 227−228.

(5) Rudnick, L. R. *Lubricant Additives: Chemistry and Applications*; CRC Press: Boca Raton, FL, 2009.

(6) Martuano, R. *The Kinetics and Mechanism of the Ene Reaction of Vinylidene Alkenes with Maleic Anhydride*; University of Sussex: U.K., 2001.

(7) Morales-Rivera, C. A.; Proust, N.; Burrington, J.; Mpourmpakis, G. Computational Screening of Lewis Acid Catalysts for the Ene Reaction between Maleic Anhydride and Polyisobutylene. *Ind. Eng. Chem. Res.* **2021**, *60*, 154−161.

(8) Poliakoff, M.; Licence, P.; George, M. W. UN Sustainable Development Goals: How Can Sustainable/Green Chemistry Contribute? By Doing Things Differently. *Curr. Opin. Green Sustainable Chem.* **2018**, *13*, 146−149.

(9) Benn, F. R.; Dwyer, J.; Chappell, I. The Ene Reaction of Maleic Anhydride with Alkenes. *J. Chem. Soc., Perkin Trans. 1* **1977**, *25*, 533−535.

(10) Thompson, M. R.; Tzoganakis, C.; Rempel, G. L. A Parametric Study of the Terminal Maleation of Polypropylene through an Alder Ene Reaction. *J. Polym. Sci., Part A: Polym. Chem.* **1998**, *36*, 2371−2380.

(11) Rondestvedt, C. S.; Wark, B. H. Mechanism of the Reaction of Mono-Olefins with Dienophiles. II. A Possible Free-Radical Mechanism. *J. Org. Chem.* **1955**, *20*, 368−372.

(12) Tiekink, E. H.; Vermeeren, P.; Bickelhaupt, F. M.; Hamlin, T. A. How Lewis Acids Catalyze Ene Reactions. *Eur. J. Org. Chem.* **2021**, *2021*, 5275−5283.

(13) Espenson, J. H. *Chemical Kinetics and Reaction Mechanisms*; McGraw-Hill, 1981.

(14) Hossain, M. D.; Ngo, H.; Guo, W. Introductory of Microsoft Excel SOLVER Function-Spreadsheet Method for Isotherm and Kinetics Modelling of Metals Biosorption in Water and Wastewater. *J. Water Sustainability* **2013**, *3*, 223−237.

(15) Adekunbi, E. A.; Babajide, J. O.; Oloyede, H. O.; Amoko, J. S.; Obijole, O. A.; Oke, I. A. Evaluation of Microsoft Excel Solver as a Tool for Adsorption Kinetics Determination. *Ife J. Sci.* **2020**, *21*, 169−183.

(16) Harris, D. C. Nonlinear Least-Squares Curve Fitting with Microsoft Excel Solver. *J. Chem. Educ.* **1998**, *75*, 119−121.

(17) Comuzzi, C.; Polese, P.; Melchior, A.; Portanova, R.; Tolazzi, M. SOLVERSTAT: A New Utility for Multipurpose Analysis. An Application to the Investigation of Dioxygenated Co(II) Complex Formation in Dimethylsulfoxide Solution. *Talanta* **2003**, *59*, 67−80.

(18) Pannetier, G.; Souchay, P. *Chemical Kinetics*; Elsevier, 1967.

(19) Abdallah, L. A. M.; Seoud, A.-L. A. Determination of the Rate Constants for a Consecutive Second Order Irreversible Chemical Reaction Using MATLAB Toolbox. *Eur. J. Sci. Res.* **2010**, *4*, 412−419.

(20) Pucci, A.; Barsocchi, C.; Rausa, R.; D'Elia, L. D.; Ciardelli, F.; D'Elia, L.; Ciardelli, F. Alder Ene Functionalization of Polyisobutene Oligomer and Styrene-Butadiene-Styrene Triblock Copolymer. *Polymer (Guildf)* **2005**, *46*, 1497−1505.

(21) Experimental data obtained in the study herein were compared to process monitoring of Lubrizol's plant reaction and found to correlate well.